Nanocluster Nucleation, Growth, and Then Agglomeration Kinetic and Mechanistic Studies: A More General, Four-Step Mechanism Involving Double Autocatalysis

Claire Besson,† Eric E. Finney, and Richard G. Finke*

Department of Chemistry, Colorado State University, Fort Collins, Colorado 80523

Received January 28, 2005. Revised Manuscript Received June 4, 2005

The discovery of the four-step, double autocatalytic mechanism by which transition-metal organometallic and metal-salt precursors self-assemble into zerovalent transition-metal nanoclusters under reductive conditions is reported. The prototype system investigated is (1,5-COD)$PtCl_2$ reduction under hydrogen plus 2 equiv of Bu_3N and 2 equiv of Proton Sponge (1,8-bis(dimethylamino)naphthalene). The reaction stoichiometry is established by TEM, XPS, NMR, and GLC. A concomitant, fast, cyclohexene hydrogenation reporter reaction is employed to monitor the kinetics of Pt^0 product/catalyst formation and agglomeration. After 15 alternative mechanisms were ruled out, a minimalistic ("Ockham's Razor") mechanism is proposed consisting of four steps: slow continuous nucleation, A → B (rate constant k_1), fast autocatalytic surface growth, A + B → 2B (rate constant k_2), bimolecular agglomeration, B + B → C (rate constant k_3), and a new, unprecedented *autocatalytic agglomeration step* between small (B) and larger, bulk-metal-like (C) particles, B + C → 1.5C (rate constant k_4). The results provide the following: a rare case of a mechanism with two autocatalytic steps in the same reaction scheme ("double autocatalysis"); the most general mechanism to date by which transition-metal nanoparticles nucleate, grow, and agglomerate to bulk metal under reductive conditions; probably the best understood self-assembly mechanism to date for such a large system in which the extensive kinetic studies required for reliable mechanistic deduction also exist; kinetic curves that can have step-function-like shapes; and insights for the synthesis of nanoclusters vs bulk-metal films (notably that higher temperature and lower concentrations favor nanocluster formation, while the opposite conditions favor bulk-metal production). A summary section details the main conclusions plus caveats and remaining questions/future research goals.

Introduction

Establishing the mechanism(s) of transition-metal nanocluster and/or bulk metal formation from, typically, simple inorganic or organometallic precursors under reductive conditions such as H_2 is an important topic in modern nanocluster science.[1] There is, however, a dearth of kinetic and mechanistic studies of modern nanocluster formation[2] and then aggregation[3] self-assembly, such studies proving difficult for primarily two reasons: (i) the lack of reproducible systems that have known stoichiometries leading to compositionally well-characterized nanoclusters which, therefore, are suitable for mechanistic studies, and especially (ii) the lack of proven methods—much less easy, routinely applied methods—which allow one to follow the kinetics of nanocluster or bulk-metal formation in real time. Due to these limitations, only a single new mechanism for transition-metal nanocluster formation under reductive conditions has appeared where the following requirements of more rigorous mechanisms have been met:[4] a well-established reaction stoichiometry is in hand, the first step of reliable mechanistic studies; compositionally well-characterized nanoclusters are studied (i.e., so that the mechanistic findings can be interpreted without error and in as great a molecular detail

* To whom correspondence should be addressed. E-mail: rfinke@lamar.colostate.edu.

† On leave from École Normale Supérieure, 45 rue d'Ulm, 75005 Paris, France, as part of a 6-month training course included in the second year of the Magistère de Chimie.

(1) (a) See our papers elsewhere[2a,b] for a comprehensive listing of the prior studies related to the mechanisms of transition-metal nanocluster formation, studies which include classic contributions from LaMer, Turkevich, Henglein, Duff, Edwards and Johnson, Glaunsinger, Hamada, and those interested in the formation of Ag^0 from Ag^+ as a part of the Ag photographic process, notably Belloni, Gavrik, Henglein, Erskov, and Fessenden. Lead references to, for example, Bawendi's or Alivisatos' studies of the mechanisms of semiconductor nanoclusters are also provided elsewhere.[3] The more recent studies of R. Tannenbaum[1b−d] on the products and mechanisms of cobalt-oxide cluster formation from $Co_2(CO)_8$ merit mention in this regard and are listed below. (b) King, S.; Hyunh, K.; Tannenbaum, R. *J. Phys Chem. B* **2003**, *107* (44), 12097. (c) Rotstein, H. G.; Tannenbaum, R. *J. Phys. Chem. B* **2002**, *106* (1), 146. (d) Tannenbaum, R. *Langmuir* **1997**, *13*, 5056.

(2) (a) Watzky, M. A.; Finke, R. G. *J. Am. Chem. Soc.* **1997**, *119*, 10382. (b) Widegren, J. A.; Aiken, J. D., III; Özkar, S.; Finke, R. G. *Chem. Mater.* **2001**, *13*, 312. (c) Aiken, J. D., III; Finke, R. G. *J. Am. Chem. Soc.* **1998**, *120*, 9545.

(3) (a) Hornstein, B. J.; Finke, R. G. *Chem. Mater.* **2004**, *16* (1), 139. (b) See also the addition/correction published in *Chem. Mater.* **2004**, *16*, 3972 which teaches an initially incorrect use of the pseudo-elementary step concept.

(4) For further discussion of the advantages incurred by treating nanocluster science by the principles of smaller molecule chemistry in-so-far as possible, but also the lower precision that one can expect for many measurements on nano- and other macro-molecules (i.e., and in comparison to conventional small molecules), see: Finke, R. G. Transition Metal Nanoclusters. In *Metal Nanoparticles, Synthesis, Characterization and Applications*; Feldheim, D. L., Foss, C. A., Jr., Eds.; Marcel Dekker: New York, 2001; pp 17−53.

10.1021/cm050207x CCC: $30.25
Published on Web 08/30/2005

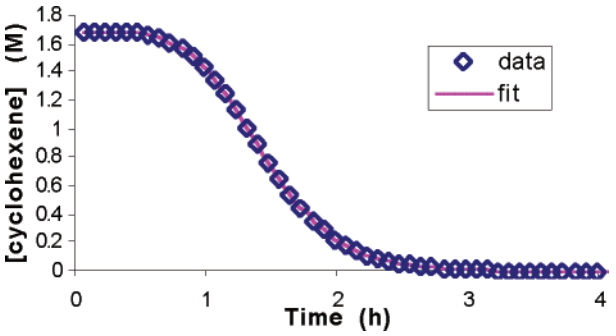

Figure 1. Prototypical cyclohexene hydrogenation curve beginning with $(Bu_4N)_5Na_3[(1,5\text{-COD})Ir{\cdot}P_2W_{15}Nb_3O_{62}]$ as the nanocluster precursor. For clarity, only one of every two experimental points obtained is displayed.

Scheme 1. The Prior[2,3] Three-Step Mechanism for Nanoparticle Nucleation, Autocatalytic Growth, and Bimolecular Agglomeration

$$A \longrightarrow B$$
$$A+B \longrightarrow 2B$$
$$2B \longrightarrow C$$

as possible[5]); detailed and extensive kinetic studies exist to support the proposed mechanism; and the resultant mechanism is expressed in terms of chemical equations (i.e., rather than just words as has been the case for many of the mechanistic proposals since the time of LaMer now over 50 years ago[2,6]).

The system that has permitted more than 700 kinetic experiments to be performed to date is Ir^0 (and other metal, vide infra) nanocluster formation. The reaction stoichiometry is firmly established, eq 1[2]

$$300[(1,5\text{-COD})Ir{\cdot}P_2W_{15}Nb_3O_{62}]^{8-} + 750H_2 \rightarrow Ir(0)_{\sim 300}(P_2W_{15}Nb_3O_{62}{}^{9-})_{\sim 66} + 300(\text{cyclooctane}) + 300H^+ + \sim 234\{P_2W_{15}Nb_3O_{62}\}^{9-} \quad (1)$$

The kinetics of the nanocluster formation have been followed indirectly, but in real time and powerfully, by the fast, catalytic amplification reaction of cyclohexene hydrogenation that is proportional to the amount of nanocluster catalyst formed.[2] For polyoxoanion-stabilized Ir^0 nanoclusters, sigmoidal kinetic curves, Figure 1, are typically observed characteristic of a two-step, minimal ("Ockham's Razor") mechanism (Scheme 1, the first two steps) consisting of slow, continuous, homogeneous nucleation (A → B, rate constant k_1), followed by fast autocatalytic surface growth (A + B → 2B, rate constant k_2)[2], where A = the nanocluster precursor ($(1,5\text{-COD})Ir{\cdot}P_2W_{15}Nb_3O_{62}{}^{8-}$ in eq 1, or (1,5-COD)$PtCl_2$ in the present work) and B = the catalytically active Ir^0 in eq 1 (or Pt^0 in the present work).

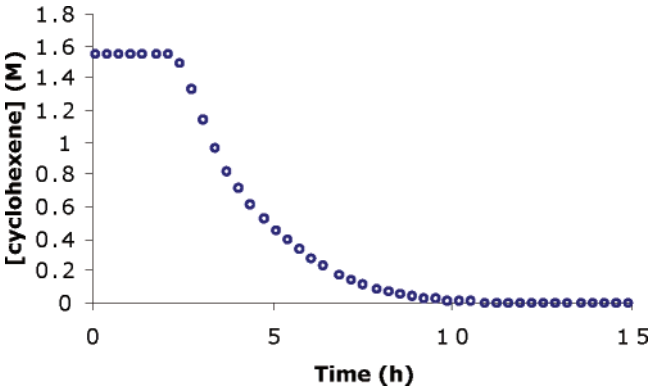

Figure 2. Typical cyclohexene hydrogenation curve obtained for (1,5-COD)$PtCl_2$ in the presence of 2 equiv each of Bu_3N and Proton Sponge. For clarity, only one out of every three experimental points actually collected is displayed in the figure.

More recently, kinetic evidence has been obtained for a third step, bimolecular agglomeration (B + B → C, rate constant k_3) in systems with added ligands such as pyridine,[3] Scheme 1. The mechanism in Scheme 1 has now been shown to apply to homogeneous nucleation[2] of organometallic precursors of Ir^I,[2] Rh^I,[7] Rh^{III},[8] as well as Ru^{II} [9] being reduced under H_2 en route to nanoclusters. It has also been shown to apply to heterogeneous (solid-surface) nucleation of Ru^{II} to Ru^0 thin-metal film formation.[9] In short, the mechanism in Scheme 1 has found broad applicability for the formation of transition-metal nanoclusters as well as bulk-metal films under reductive conditions.

The Case of Pt Nanoclusters. Of considerable interest and current effort are nanoclusters of[10] Pt due to the high catalytic activity and the wide range of reactions catalyzed by Pt metal particles. For some time now, we have known that Pt precursors to nanoclusters or bulk metal (i.e., and under the conditions employed, vide infra), as well as our pyridine-ligated Ir^I precursor to Ir^0 nanoclusters (and thus by implication presumably many other systems where ligands are present), *do not* follow the three-step mechanism in Scheme 1. *This important fact is completely unappreciated in the literature of Pt (or other relevant metal) nanoclusters.* Moreover, the extant Pt nanocluster literature[10] erroneously implies that it is routine to synthesize stable Pt nanoclusters without the formation of bulk metal. What follows suggests that this is generally not true.

Figure 2 shows a typical kinetic curve for what will be the prototype system studied herein, (1,5-COD)$PtCl_2$ reduction under hydrogen in the presence of 2 equiv of Bu_3N and

(5) For example, see elsewhere for a case where kinetic studies of compositionally well-characterized nanoclusters has allowed a model of how tridentate ligands appear to preferentially bind to the {111} facets of selected nanocluster surfaces: Finke, R. G.; Özkar, S. *Coord. Chem. Rev.* **2004**, *248* (12), 135.

(6) (a) LaMer, V. K. Dinegar, R. H. *J. Am. Chem. Soc.* **1950**, *72*, 4847. (b) LaMer, V. K. *Ind. Eng. Chem.* **1951**, *19*, 482. (c) LaMer's mechanism was for *sulfur sol*, and not transition-metal, formation; it consists of *burst nucleation* from supersaturated solution, $nS \rightarrow S_n$, followed by *diffusion-controlled agglomerative growth*, $S_n + S \rightarrow S_{n+1}$. Note that LaMer's mechanism is completely different from the mechanism for transition-metal nanocluster (slow, continuous) nucleation, then (nondiffusion controlled) autocatalytic surface growth published in 1997.[2] LaMer's mechanism is also completely different from the expanded, more general mechanism published herein for transition-metal nanocluster formation and then agglomeration under reductive conditions.

(7) (a) Aiken, J. D., III; Finke, R. G. *Chem. Mater.* **1999**, *11*, 1035. (b) Widegren, J. A.; Finke, R. G. *Inorg. Chem.* **2002**, *41*, 1558.

(8) Weddle, K. S.; Aiken, J. D., III; Finke, R. G. *J. Am. Chem. Soc.* **1998**, *120*, 5653.

(9) Widegren, J. A.; Bennett, M. A.; Finke, R. G. *J. Am. Chem. Soc.* **2003**, *125*, 10301.

(10) (a) Rampino, L. D.; Nord, F. F. *J. Am. Chem. Soc.* **1941**, *63*, 2745. (b) Hirai, H.; Nakao, Y.; Toshima, N. *J. Macromol. Sci.-Chem.* **1979**, *A13*, 727. (c) de Caro, D.; Bradley, J. S. *New J. Chem.* **1998**, *22*, 1267. (d) Rodriguez, A.; Amiens, C.; Chaudret, B.; Casanove, M.-J.; Lecante, P.; Bradley, J. S. *Chem. Mater.* **1996**, *8*, 1978. (e) Bönnemann, H.; Waldöfner, N.; Haubold, H.-G.; Vad, T. *Chem. Mater.* **2002**, *14*, 1115.

2 equiv of Proton Sponge (1,8-bis(dimethylamino)naphthalene) plus the concomitant reporter reaction of cyclohexene hydrogenation. The unusual kinetic curves, Figure 2, are step-function-like; their appearance is as if one forgot to add a reagent or stir the system until the point at which the reaction takes off after a 0.44−3.0 h induction period! In fact, all reagents are present, the solutions are well-stirred, and the observed curves are reproducible within the cited range of the induction period (the variability of which[11] will be examined in some detail later in the paper).

The exact reaction and mechanism underlying these kinetic curves is of interest for multiple reasons: (i) because of the unusual shape of the curves (What mechanism can account for this? Can such curves be fit and understood quantitatively? What new insights result?); (ii) because the results promise to be highly relevant to the synthesis of Pt, Ir, Ru, possibly Pd, and any other transition-metal nanocluster systems showing curves such as the one in Figure 2; and (iii) since it appears, upon reflection and at least intuitively, as if larger metal particles have to be formed before the catalysis "takes off", a situation exactly opposite to the expected higher reactivity of the smaller, more energetic, and higher surface-area nanoclusters.[3] Or is some other explanation responsible for the long induction periods?

Herein, we report the full details of our studies of (1,5-COD)Pt^{II} placed under H_2 and followed by the cyclohexene hydrogenation, catalytic amplification/reporter reaction kinetic method.[2,3,7−9,11] The results are most interesting and (a) show that kinetic curves such as those in Figure 2 are characteristic of a reaction that produces nanoclusters plus bulk metal, (b) reveal a mechanism involving nanocluster intermediates (as in Scheme 1 above) plus the added autocatalytic step of B + C → 1.5C (B = nanoclusters, C = bulk metal) and, in the more general case, probably also participation by A + C → 1.5C, and (c) show that this mechanism accounts *quantitatively* for the unusual, approaching step-function-like nature of the curves. The results also (d) lead to the postulate of a previously little appreciated size-dependent M−L (M = metal; L = ligand) bond dissociation energy, BDE (in which larger particles have a lower M−L BDE) so that only the larger, bulk-metal-like particles can dissociate sufficient coordinated ligand to become coordinatively unsaturated and, therefore, catalytically active. In addition, the results (e) provide insights into how to best synthesize Pt, Ir, and other transition-metal nanoclusters under conditions where they follow the more general mechanism detailed herein. A preliminary account of the present work has appeared.[12] The present full paper provides many additional, previously unpublished results and insights.

Experimental Section

(1) Materials. Unless indicated otherwise, all commercially available solvents, compounds, and materials were used as received. Acetone, purchased from Burdick and Jackson (water content <0.2%), was purged with argon for at least 20 min before being stored in a nitrogen atmosphere drybox where it was used. The NMR solvent CD_2Cl_2 (D, 99.9%) was purchased from Cambridge Isotope Laboratories. Cyclohexene (Aldrich, 99%) and tributylamine (J. T. Baker Chemicals) were both purified by distillation over sodium under argon and stored in the drybox. Hydrogen gas (General Air, 99.5%) was used as received. Dichloro-1,5-cyclooctadieneplatinum(II) was purchased from Strem Chemicals and stored in the drybox. Proton Sponge (1,8-bis(dimethylamino)naphthalene) (Aldrich, 99%) was also stored in the drybox. Pyridine (Aldrich 99%) was distilled under vacuum and stored in the drybox over 4 Å activated molecular sieves. Stock solutions of tributylamine and pyridine were prepared and stored in the drybox; the tributylamine solution (4.2×10^{-2} M) was prepared by mixing 0.1 mL of tributylamine and 9.9 mL of acetone (volumes measured with a syringe); the pyridine solution (1.8×10^{-2} M) was prepared by adding 73 μL of pyridine to a volumetric flask and diluting to 50 mL with acetone. The Ir^0 nanocluster precursor $(Bu_4N)_5Na_3[(1,5\text{-}COD)Ir{\cdot}P_2W_{15}Nb_3O_{62}]$ was prepared according to our literature[13] and its purity checked by ^{31}P NMR.

(2) Nanocluster Formation and Cyclohexene Hydrogenation Apparatus. All reactions were carried out in our previously described,[2,11] custom-built pressurized hydrogenation apparatus consisting, briefly, of a Fischer-Porter (F-P) bottle connected via Swagelock TFE-sealed Quick-Connects to a H_2 line and a Omega PX-621 pressure transducer interfaced to a PC using LabVIEW 6.1.

(3) (1,5-COD)$PtCl_2$ and Other Organometallic Reductions and Concomitant Cyclohexene Hydrogenation Reactions. *(i) Standard Conditions Beginning with (1,5-COD)$PtCl_2$.* The starting materials 1.5 mg (4.0 μmol) (1,5-COD)$PtCl_2$ and 2 equiv of Proton Sponge (1.7 mg) were weighed into a two-dram glass vial. Two equivalents of Bu_3N (8.0 μmol, 0.19 mL of a 0.0420 M solution in acetone) and 2.5 mL of acetone were added to the vial via a gastight syringe. The solution was then mixed with a disposable polyethylene pipet until it was homogeneous. Next, the solution was transferred using the pipet into a new 22 × 175 mm Pyrex culture tube with a new 15.9 × 9.1 mm Teflon-coated stir bar. Then, 0.5 mL (4.94 mmol) of cyclohexene was added via a gastight syringe.

The culture tube was then placed in the Fisher-Porter (F-P) bottle that is part of the overall apparatus described in section (2) above. The bottle was sealed, brought out of the drybox, and then attached to the hydrogenation apparatus via the Swagelock TFE-sealed Quick-Connects. The bottom of the bottle was immersed in a water-filled jacketed reaction flask attached to a recirculating water bath maintained at 22.0 ± 0.1 °C. Vortex stirring was initiated using a Fischer jumbo magnetic stirrer and the F-P bottle was purged with 40 psig of H_2 13 times (15 s per purge). At 5 min, the valve between the F-P bottle and the hydrogen tank was closed and the data collection initiated. The pressure was recorded every 2.5 min yielding, typically, 200-1500 data points of ±0.01 psig precision.

The short-time H_2 vs time pressure data were corrected as before[2b,3,9] for solvent-vapor pressure and any nonequilibrium temperature conditions by back-extrapolating from the maximum pressure recorded[2b] (the induction period is long enough to allow the system to reach equilibrium before any hydrogen uptake begins, thereby allowing a reliable back-extrapolation). The raw H_2 pressure data was collected, pasted into Excel, and then worked up by converting it into cyclohexene concentration data via the known 1:1 H_2 to cyclohexene stoichiometry[11] (eq 2, vide infra). GLC

(11) (a) Lin, Y.; Finke R. G. *J. Am. Chem. Soc.* **1994**, *116*, 8335. (b) Lin, Y.; Finke, R. G. *Inorg. Chem.* **1994**, *33*, 4891.
(12) Besson, C.; Finney, E. E.; Finke, R. G. *J. Am. Chem. Soc.* **2005**, *127*, 8179.
(13) (a) Hornstein, B. J.; Finke, R. G. *Inorg. Chem.* **2002**, *41*, 2720. (b) Pohl, M.; Lyon, D. K.; Mizuno, N.; Nomiya, K.; Finke, R. G. *Inorg. Chem.* **1995**, *34*, 1413.

control experiments confirmed that, in the present case, no cyclohexene remained at the end of a typical reaction. The initial concentration of cyclohexene was calculated from the total pressure loss and this experimental cyclohexene initial concentration was used in all further calculations. Numerical integration of the resultant data was carried out using the freeware MacKinetics.[14]

(ii) Standard Conditions Beginning with $(Bu_4N)_5Na_3[(1,5\text{-COD})Ir{\cdot}P_2W_{15}Nb_3O_{62}]$. These reactions were carried out as described in our previous literature.[2,3]

(4) ^{1}H NMR Studies Following the Loss of (1,5-COD)PtCl$_2$. The importance of this NMR experiment, and the GLC one which follows, is that they allow a closer-to-direct monitoring of the conversion of (1,5-COD)$PtCl_2$ into cyclooctane and, by mass balance (Scheme 3, vide infra), Pt^0 products. A Standard Conditions reaction beginning with (1,5-COD)$PtCl_2$ was prepared as in (3)(i), except that the reaction was scaled up by a factor of 3 by tripling all reagents. Four samples for NMR analysis were taken, one every 30 min, via the following procedure: first, the gas-regulator valve between the F-P bottle and the hydrogen tank was opened. Next, the top ball valve of the F-P bottle was opened under the resultant continuous flow of H_2. A sample (1.8 mL) was then removed through the top of the F-P bottle using a gastight syringe equipped with a 30 cm long needle, the sample was placed in a 5 mL vial, and the F-P bottle was then closed via its top ball valve. After the 10 s necessary for the pressure to return to ca. 40 psig, the valve to the hydrogen tank was also closed. The total operation took less than 1 min. The sample was then bought into the drybox and dried under vacuum overnight. Benzaldehyde (0.8 μL, 4.7 μmol) was added as an internal standard via a gastight syringe. The solid was dissolved in 1 g of CD_2Cl_2 and the resulting solution was transferred into a Spectra Tech NMR tube (5 mm o.d.) using a disposable polyethylene pipet. Spectra were recorded at room temperature on a Varian Inova 300 MHz instrument (relaxation delay 1 s, pulse 38.9° acquisition time 2.732 s, width 6000 Hz, 32 repetitions). Chemical shifts were referenced at 0 ppm vs internal TMS. ^{1}H NMR (300 MHz, CD_2Cl_2) (1,5-COD)$PtCl_2$: δ 5.48 (t, J = 33 Hz, 4H, =CH), 2.60 (m, 4H, *endo*-CH_2), 2.15 (m, 4H, *exo*-CH_2). C_6H_5-CHO: δ 9.93 (s, 1H, CHO), 7.80 (m, 2H, *o*-H), 7.58 (m, 1H, *p*-H), 7.58 (m, 1H, *p*-H), 7.56 (m, 2H, *m*-H). Since the aromatic region and 0 and 4 ppm regions of the spectrum were obscured by traces of nonevaporated species (i.e., Proton Sponge), the peaks used for the evaluation of the concentration were the triplet at 5.48 ppm for (1,5-COD)$PtCl_2$ and the singlet at 9.93 ppm for benzaldehyde.

(5) GLC Studies Following the Loss of (1,5-COD)PtCl$_2$ by Monitoring the 1,5-COD Plus H_2 to Cyclooctane Conversion. A Standard Conditions reaction beginning with (1,5-COD)$PtCl_2$ was prepared as in (3)(i), except that all quantities were tripled. Samples for GLC analysis were taken via the following procedure: first, the gas-regulator valve between the F-P bottle and the hydrogen tank was opened. Next, the top ball valve of the F-P bottle was opened to allow a continuous H_2 flow through the F-P bottle and out its top valve. A sample (about 0.1 mL) was then removed with a gastight syringe equipped with a 30 cm long needle, the sample was placed in a 1 mL vial, and the F-P bottle was closed via its top ball valve. After the 10 s necessary for the pressure to return to ca. 40 psig, the valve to the hydrogen tank was also closed. The total operation took less than 1 min. The sample was analyzed immediately by gas-liquid chromatography performed on a Hewlett-Packard HP-5890 equipped with a Supelco SPB-1 capillary column (30 m × 0.25 mm), a flame ionization detector and interfaced to a PC using Galaxie Chromatography Data System software, version 1.7.403.22. The injector temperature was 180 °C and the detector 200 °C. The following temperature program was used: 35 °C for 4 min, ramping up at 15 °C/min to a final temperature of 200 °C, which was then maintained for 1 min. Under these conditions, the respective retention volumes (and the corresponding retention times under a flow rate of 0.9 mL/min) of acetone, cyclohexane, cyclohexene, and cyclooctane are 1.9 mL (2.1 min), 3.2 mL (3.6 min), 3.6 mL (4.0 min), and 8.0 mL (8.9 min), respectively. The conversion of area to millimoles of cyclooctane was performed using a five-point calibration curve constructed using authentic samples. Since the retention time of cyclooctadiene is also 4 min on this column and with this temperature program, additional experiments were done with a Supelcowax-10 column (30 m × 0.25 mm, 0.25 μm film) with the same temperature program. The retention volumes of cyclohexane, cyclohexene, acetone, cyclooctane, and cyclooctadiene (and the corresponding retention times under our flow rate of 0.5 mL/min on the Supelcowax-10 column) are, respectively 1.1, 1.3, 1.4, and 2.8 mL (2.2, 2.6, 2.8, 5.6, and 8.2 min). No unreduced cyclooctadiene was detected (detection limit of $\geq$0.2 mM).

(6) Transmission Electron Microscopy (TEM). The reaction was carried out as described in the Standard Conditions section (3)(i), except that all quantities were tripled. About 5 min after the first sign of pressure decrease, the gas-regulator valve to the hydrogen tank was opened and the hydrogen was allowed to flow through the F-P bottle whose top valve was also opened. The solution had changed from colorless to homogeneous light gray at this time. About 2 mL of the solution was syringed in a 5 mL glass vial. The vial was then capped and immediately frozen by immersing it into liquid nitrogen. The vial and its frozen solution were brought into the drybox, by which time (an additional ca. 5 min) the solution had already melted in the antechamber of the drybox. Two drops of the solution were placed on a TEM grid using a disposable polyethylene pipet (the TEM grids used were silicon monoxide type-A, Formvar backing, 300 mesh, copper grids from Ted Pella, Inc.). The solvent quickly evaporated and the grid was sealed in a vial and sent for analysis to the University of Oregon, where TEM was performed by Dr. JoAn Hudson and her staff.

Since nanoclusters as artifacts can be formed in the TEM beam from at least some organometallic precursors[15] (i.e., and if any of that precursor remains as the end of a nancluster formation reaction), a control was done to test whether nanoclusters can be formed in the TEM beam from (1,5-COD)$PtCl_2$. Specifically, a drop of an acetone solution of (1,5-COD)$PtCl_2$, Proton Sponge, and Bu_3N was placed on a TEM grid and analyzed by TEM. No nanoclusters were found, indicating that the observed nanoclusters are formed in the reduction reaction, not in the TEM beam on the TEM grid.

(7) X-ray Photoelectron Spectroscopy (XPS). At the end of a reaction conducted as indicated in the Standard Conditions reaction (3)(i), the Pyrex culture tube used as a liner inside the F-P bottle was broken and the black layer on the wall of a ca. 1 × 1 cm piece of that reaction tube was analyzed by XPS. The spectrum was collected using a Physical Electronics (PHI) Model 5800XPS system equipped with a monochromator (Al Kα source, $h\nu$ = 1486.8 eV; system pressure $\leq 5 \times 10^{-9}$ Torr = 6.7×10^{-7} Pa) and a

(14) Leipold, W. S., III. http://members.dca.net/leipold/mk/advert.html.

(15) (a) TEM-induced artifacts are certainly well-established in the literature (see p 6 and ref 3 elsewhere[15b]). Our[15c] and others[15d] experiences seem to be that second-row (e.g., Rh[15c,d]) nanoclusters are often labile in the TEM beam while third-row metals (e.g., Ir) appear stable,[11] at least under the TEM conditions we have tended to employ and on the basis of multiple TEM control experiments performed when we first started using TEM.[11] (b) Aiken, J. D., III; Finke, R. G. *J. Mol. Catal. A: Chem.* **1999**, *145*, 1−44 (see p 6 and the references cited in ref 3). (c) Hagen, C.; Widegren, J. A.; Maitlis, P. M.; Finke, R. G. *J. Am. Chem. Soc.* **2005**, *127*, 4423−4432. (d) Jaska, C. A.; Manners, I. *J. Am. Chem. Soc.* **2004**, *126*, 9776.

hemispherical analyzer to detect the ejected electrons. The results confirmed the black product on the walls of the reaction tube is the expected Pt^0 via the good agreement of the observed binding energies (vs the literature[16,17] listed in parentheses): 520 eV ($4p_{3/2}$, 519.5−519.8 eV), 333 eV ($4d_{3/2}$), 314 eV ($4d_{5/2}$, 314.2−314.6), 74.7 eV ($4f_{5/2}$, 74.2−74.5), 71.3 eV ($4f_{7/2}$, 70.8−71.3). The spectrum, Figure S-1, and an enlargement of the 4f peaks, Figure S2, are provided in the Supporting Information.

(8) MacKinetics Numerical Integration. The numerical integrations were carried out using the free software MacKinetics (version 0.9.1b, by Walter S. Leipold III; on-line information obtainable at http:// members.dca.net/leipold/mk/advert.html). First, when the data were being fit with species C (the agglomerated, bulk metal; see eqs 4 and 5) as the catalyst, the H_2 loss data were converted to *[cyclohexene]* and then to *1/2([cyclohexene]$_0$ – [cyclohexene])* data. The following procedure then was used to avoid the well-known problem[18] of finding local minima, rather than the desired true global minimum, of the parameters surface vs the residual (which indicates the difference between the experimental and calculated curves). For each new type of reaction, an extended scan of the surface was first performed as follows: during a typical grid search, each of the four kinetic parameters (k_1−k_4) was varied over 3 orders of magnitude by using 10 equally spaced search points within that 10^3 range for each parameter. If the best result of a grid search (i.e., the set of parameters, among the 10 000 checked, that gives the smallest residual) had one or more parameter that landed at one of the limiting values of the grid, then the grid was shifted and the search was performed again until the resulting, new set of best parameters lay *between* the search limits. Then, the following procedure was carried out for all the grid search results: the values from the first grid search were used as the initial guess for the predictor/corrector program of MacKinetics. The resulting new set of values was then once again used as a new initial guess and the process iterated until the results were self-consistent as judged by those final, acceptable parameters all being within $\leq\pm$100% of the prior iteration (except for k_1, which showed a greater variation; the error bars associated with a global search of a five-dimensional space will be discussed in the Results and Discussion section). As a control to verify that the resulting grid search parameters are really the global minimum, the same iterative process was carried using initial guesses taken within at least 1 order of magnitude of the earlier "best" result for each parameter. In some cases, notably data set Trial #1 in Table 1 of the Results and Discussion section, this procedure resulted in a sizable number of total searches, 34 in that case (see Table 1). Residuals were typically 0.008−0.01 for the kinetic curve fits reported herein (residuals of even $\leq$0.02 corresponded to visually good fits).

(9) Mapping of the Five-Dimensional, Residual vs Parameters Space. Instead of recording only the best result of a grid search (the final set of parameters that gives the closest fit), it is possible to keep the results of all estimates, typically 10 000 (10 values over a range of 3 orders of magnitude for each parameter). These 10 000 points give a complete five-dimensional mapping of the part of the surface included in the limits of the chosen grid. The display of such a five-dimensional map in three dimensions is of course impossible. However, it is possible to reduce it to three-dimensional maps by keeping two parameters constant at a chosen value (we picked their best-fit values) and then varying two others; 600 different maps can be drawn in this manner, 2 of which are provided in Figure 8 of the main text and 4 more are provided in Figures S-17 to S-20 of the Supporting Information.

(10) Numerical Simulations. Simulations were carried out to obtain a better physical intuition for the effects on the kinetic curves of changing the rate constants k_1−k_4 or the initial concentration of precursor A. For convenience, the simulations were carried out with the observed parameters and the cyclohexene initial concentration as $[A]_0$ so that the resultant calculated concentrations are 1200 times the real ones—a convenient scaling which, of course, does not affect the relative A, B, and C concentrations. A standard curve was generated and plotted using the following parameters: $k_{1,obs} = 10^{-5}$ h^{-1}, $k_{2,obs} = 4.5$ M^{-1} h^{-1}, $k_{3,obs} = 0.2$ M^{-1} h^{-1}, $k_{4,obs} = 0.7$ h^{-1} M^{-1}, $[A]_0 = 1.6$ M. Then, five sets of curves were generated and plotted by varying one of the parameters at a time ($k_{1,obs} = 10^{-10}$, 10^{-9}, 10^{-8}, 10^{-7}, 10^{-6}, 10^{-5}, 10^{-4}, 10^{-3}, 10^{-2}, 10^{-1}, 1 h^{-1}; $k_2 =$ 0.001, 0.01, 0.1, 1, 2, 3, 4, 4.5, 5, 6, 7, 8, 10, 50, 100 M^{-1} h^{-1}; $k_3 =$ 0.001, 0.01, 0.1, 0.15, 0.2, 0.25, 0.3, 0.4, 0.5, 1, 10, 50 M^{-1} h^{-1}; $k_4 =$ 0.001, 0.01, 0.1, 0.3, 0.5, 0.6, 0.65, 0.7, 0.75, 0.8, 0.9, 1, 10, 50, 100 M^{-1} h^{-1}; $[A]_0 =$ 0.2, 0.4, 0.6, 0.8, 1.0, 1.2, 1.4, 1.6, 1.8, 2.0, 2.2, 2.4 M). The results of these simulations are provided in Figures S-21 to S-25 and are discussed in the main text.

Results and Discussion

(1) Pt Conversion Reaction Stoichiometry. The main system examined herein is the reduction of (1,5-COD)$PtCl_2$ in the presence of 2 equiv of tributylamine and 2 equiv of PS (1,8-bis(dimethylamino)naphthalene, a strong, noncoordinating base added to scavenge the 2 H^+ formed from the H_2 reduction of Pt^{II}, Scheme 2. Concomitant cyclohexene reduction serves as the reporter reaction for the Pt^0 formed, as also shown in Scheme 2. The course of a typical Pt^0 formation and concomitant cyclohexene hydrogenation reaction is as follows: a clear, colorless solution of the precursor (1.34 mmol L^{-1}) and cyclohexene (1.65 mol L^{-1}) in acetone is pressurized with 40 psig hydrogen. No hydrogen consumption is observed during a 0.4−3.0 h induction period that averages ∼1.4 h, but a *sudden* uptake of hydrogen then takes place (as shown back in Figure 2) at the same time the solution becomes a gray, then cloudy-black suspension, indicative of the formation of nanoclusters and suspended bulk metal.

Scheme 2. Observed (1,5-COD)$PtCl_2$ Reduction and Concomitant Cyclohexene Conversion Stoichiometries for a Standard Conditions Reaction in the Presence of 2 equiv of Bu_3N and 2 equiv of Proton Sponge and at an Initial Pressure of 40 psig H_2

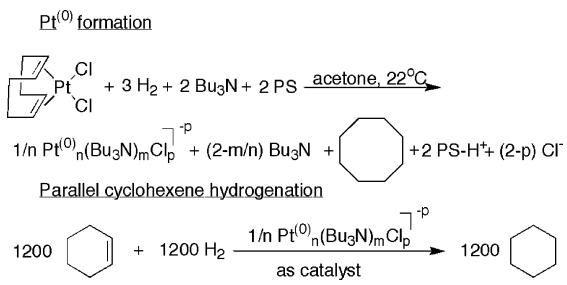

TEM of a couple of drops of solution taken within 5 min of the end of the induction period shows the presence of 40

(16) Moulder, J. F.; Stickle, W. F.; Sobol, P. E.; Bomben, K. D. *Handbook of X-ray Photoelectron Spectroscopy;* Physical Electronics, Inc.: Eden Prairie, MN, 1995.

(17) NIST Photoelectron Spectroscopy Database, NIST Standard Reference database 20, Version 3.4 (Web Version), http://srdata.nist.gov/xps/index.htm.

(18) The following book on numerical analysis methods notes on p 387, in their chapter on minimization or maximization of functions, the fact that "Finding a global extremum is, in general, a very difficult problem": Press, W. H.; Teukolsky, S. A.; Vetterling, W. T.; Flannery, B. P. *Numerical Recipes in Fortran: The Art of Scientific Computing*, 2nd ed.; Cambridge University Press: Cambridge, 1992.

± 10 Å nanoclusters, Figure 3, corresponding *on average* to $Pt^0_{\sim 2200}$. GLC experiments show that the hydrogenation of cyclooctadiene to give cyclooctane parallels the cyclohexene hydrogenation. In particular, the length of the induction period is exactly the same for cyclooctadiene hydrogenation monitored by GLC and the cyclohexene hydrogenation used to follow the Pt^0 formation indirectly. After 10−20 h, the cyclohexene hydrogenation is complete (GLC experiments confirm that no cyclohexene remains) and the reaction solution is again colorless with particles of black bulk Pt^0 metal (verified by XPS) visible in the solution, on the stir bar and on the walls of the reaction tube. Back of the envelope calculations, based on the fact that the Pt^0 particles are visible by eye, implies a size of 0.1 mm (i.e., 0.003 rad when viewed at 25 cm[19]), corresponding to bulk platinum metal with an *upper limit* of less than ca. 10^{11} atoms per particle.

(2) Kinetic Studies Following the H_2 Pressure Loss. A typical curve for the reduction of (1,5-COD)$PtCl_2$ and, concomitantly, cyclohexene in the presence of 2 equiv each of Bu_3N and Proton Sponge is provided in Figure 4 along with an attempt to fit it by our prior two- or three-step mechanisms summarized back in Scheme 1. For convenience, all hydrogen loss pressure data have been converted into the equivalent cyclohexene loss concentration data, using the ideal gas law and following the known[2,11] stoichiometry of the hydrogenation reaction, eq 2. That the stoichiometry in eq 2 is obeyed in this case, as before,[2] was verified by showing that the H_2 loss matches the moles of cyclohexene consumed by GLC. Note that the hydrogen loss due to the reduction of the cyclooctadiene ligand of the precatalyst is negligible given the 1200:1 ratio of the cyclohexene to Pt precursor concentrations. The kinetic curve shown in Figure

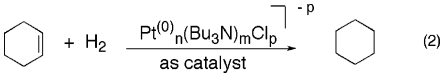

4 has been repeated 29 times (including TEM and GLC vs time experiments) without discernible variation of the observed global shape. Note that a *very sudden* cyclohexene loss/H_2 uptake and a curve *without an inflection point* is seen following the 1.4 h average induction period-a step-function like curve, one distinctly different than the smoother, less-sudden curve involving an inflection point seen previously (cf. Figures 2 and 4 vs Figure 1).

Significantly, neither our prior two-step or three-step mechanisms can fit the new kinetic curves exemplified by Figure 4. *This is an important observation; it means that a new mechanism for nanoparticle formation has been discovered.* This statement follows since the existing, kinetically documented, previously most general mechanism for transition-metal nanoparticle formation and then agglomeration is the three-step mechanism in Scheme 1.[2,3] Given the rather broad applicability of even the prior two- and three-step mechanisms,[2,3,7−9,11,13] one's first guess is that the addition of one or more new, previously unappreciated steps of the prior two- or three-step mechanism back in Scheme 1 is the essence of this finding. Below we demonstrate that *only by the inclusion of two autocatalytic steps* can the kinetic curve in Figure 4 be well-fit, a rare example of double autocatalysis in a single reaction scheme.[20]

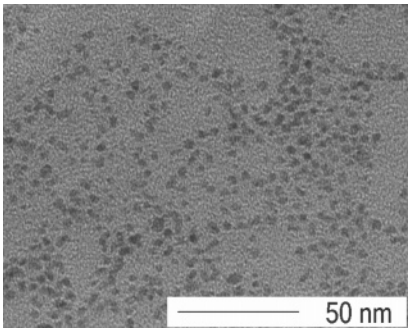

Figure 3. Representative TEM image of Pt^0 nanoclusters formed during the induction period of the hydrogenation of (COD)$PtCl_2$. The average size of the nanoclusters is 40 ± 10 Å (567 particles counted).

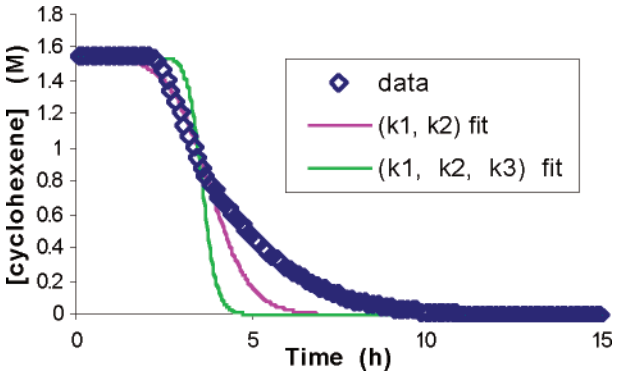

Figure 4. A typical (1,5-COD)$PtCl_2$ reduction and concomitant cyclohexene hydrogenation curve plus attempted curve fits using the established two-step [A → B, A + B → 2B (k_1, k_2)] and three-step [A → B, A + B → 2B, 2B → C (k_1, k_2, k_3)] mechanisms. The gross failure of the known mechanisms[2,3] to fit the data requires, in turn, that a new mechanism has been discovered.

Scheme 3. Proposed Four-Step, Double Autocatalytic Mechanism in Graphic Form[a]

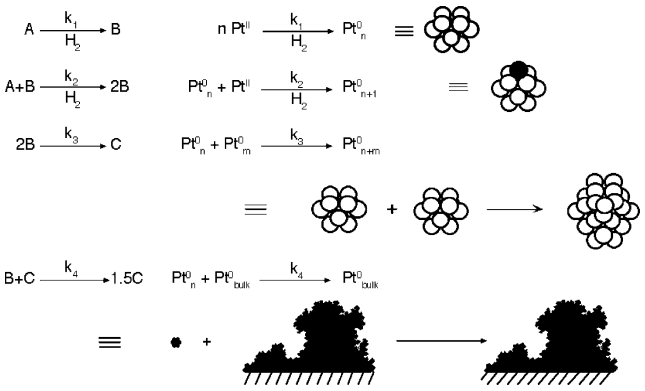

[a] The exact form and size of the "bulk" metal illustrated schematically in the k_4 step is not known better than the $<10^{11}$ Pt^0 atoms size implied by its visibility to the naked eye and the back-of-the-envelope calculation provided earlier.

(3) Proposed Mechanism and Pseudo-elementary Step Treatment of the Kinetics and the Cyclohexene Hydrogenation Reporter Reaction. The proposed, four-step minimalistic ("Ockham's Razor") mechanism is shown in eqs 3a−3d and Scheme 3. In this mechanism, A is the precursor

(19) Welford, W. T. *Geometrical Optics;* North-Holland Publishing Company: Amsterdam, 1962; p 115.

((1,5-COD)$PtCl_2$ in the present case), B represents *inactive* nanoclusters, and C is the catalytically *active* bulk metal, eq 4. The new, novel step in the mechanism is the B + C →

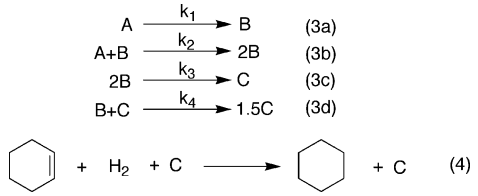

1.5C step, an *autocatalytic agglomeration step*. The reader will note that the stoichiometry factor of 1.5 is exactly true only for the initial agglomeration; in later steps for larger C particles this factor approaches 1.0. However, the curve fits were not improved using a factor, β, closer to 1 as documented by the attempted fits with other β values provided in the Supporting Information. We also know from our prior work[2] that the mathematics of the autocatalytic function still hold true for the more general case appropriate to this work of $1 < \beta < 1.5$.[21] It is important to note that the proposed mechanism is the result of a lengthy process of ruling out 15 conceivable alternative mechanisms, including one where B is the active catalyst, vide infra.

(4) Pseudo-elementary Step Treatment of the Kinetic Data. The stoichiometric ratio of cyclohexene to precatalyst, A, of 1200:1 indicates that, *on average*,[22] each catalytic metal atom reacts 1200 times and thus gives 1200 cyclohexane molecules. The pseudo-elementary step concept[2]—that is, the addition of the fast cyclohexene hydrogenation catalytic reporter reaction to the slow reactions producing the catalyst C—enables us to write eqs 5a−5d and to make the needed, critical link of $[C]_t$ to [cyclohexene]$_t$, via the pseudo-elementary step eq 5d: With eq 5d in hand, one can in turn

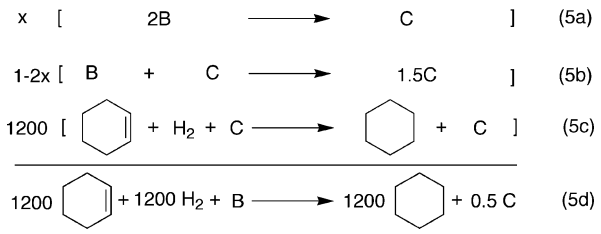

write the needed differential equation, eq 6a, and its integrated form, eq 6b (details of the needed derivation are provided in the Supporting Information; our earlier work can also be consulted for those interested in learning more about the pseudo-elementary step concept, its correct usage,[2,3] and the approximations underlying its use; see ref 22 elsewhere[3]):

$$-\frac{1}{1200}\frac{d[\bigcirc]}{dt} = \frac{1}{0.5}\frac{d[C]}{dt} \qquad (6a)$$

$$\frac{1}{2}\left([\bigcirc]_0 - [\bigcirc]\right) = 1200\,[C] \qquad (6b)$$

The resultant proportionality in eq 6b allows one to curve fit the *cyclohexene* loss data yet derive the desired rate constants for the four *slower nanocluster formation and agglomeration steps*, k_1-k_4. In actual practice, it is convenient to fit the data to 1/2([cyclohexene]$_0$-[cyclohexene]). As a consequence, the observed values of the rate constants $k_{1,obs}$, $k_{2,obs}$, $k_{3,obs}$, and $k_{4,obs}$ differ from the microscopic k_1, k_2, k_3, and k_4 by the straightforward correction factors shown in eq 7 of 1200 for all but $k_{1,obs}$ (see the Supporting Information for the full details of the needed derivations). A typical—excellent—curve fit accomplished using MacKinetics, in which the fitted line is indistinguishable from the data, is presented in Figure 5.

$$\left.\begin{aligned} k_1 &= k_{1,obs} \\ k_2 &= 1200\ k_{2,obs} \\ k_3 &= 1200\ k_{3,obs} \\ k_4 &= 1200\ k_{4,obs} \end{aligned}\right\} \qquad (7)$$

(4) GLC and ^{1}H NMR Verification of the Cyclohexene Reporter Reaction and Pseudo-elementary Step Approach Used To Follow the Nanocluster Formation and Agglomeration Kinetics. Previously, in the case of the two-step mechanism we used GLC to verify the indirect cyclohexene reporter reaction kinetic method and as a check on all its associated mathematics and derivations.[2] Verification of the indirect kinetic method in the present case was deemed important as well; hence, ^{1}H NMR and GLC studies were used to provide a direct (^{1}H NMR), to approaching direct (GLC), monitoring of the loss of the (1,5-COD)$PtCl_2$ precursor.

The loss of (1,5-COD)$PtCl_2$ monitored by ^{1}H NMR yields only a limited number of points, but still provides a direct confirmation of the step-function-like nature of the curve, Figure 6. GLC monitoring of the formation of cyclooctane, from hydrogenation of the cyclooctadiene ligand on the precursor, (1,5-COD)$PtCl_2$ (recall the reaction's stoichiometry provided back in Scheme 2), yielded additional data,

(20) *Theoretical* descriptions of double autocatalysis in the same net reaction scheme began with Lotka in 1920[20a] and have reappeared in attempts to explain cooperativity and self-regulation of ATPase pumps.[20b] However, so far we have been able to find *only three prior experimental examples*:[20c,d] (a) Lotka, A. J. *J. Am. Chem. Soc.* **1920**, *42*, 1595. (b) Weissmuller, G.; Bisch, P. M. *Eur. Biophys. J.* **1993**, *22* (1), 63. (c) Two examples from oscillating reactions: Epstein, I. R.; Pojman, J. A. *An Introduction to Nonlinear Chemical Dynamics. Oscillation, Waves, Patterns and Chaos*; Oxford University Press: Oxford, 1998; p 98. (d) An example involving nitrile hydrolysis: Izzo, B.; Harrell, C. L.; Klein, M. T. *AIChE J.* **1997**, *43* (8), 2048.

(21) We have previously treated this issue, in the case of our Ir^0 nanocluster system, namely, that the step there of A + B → 2B is, in the general case and for that system, actually A + $Ir^{(0)}_n$ → $Ir^{(0)}_{n+1}$; hence, the stoichiometry factor of 2 is, in the more general case, actually a "scaling factor" of $(1 + x_{growth})/2$ introduced elsewhere to deal with this issue in an average way.[2] In the present work, the failure to derive improved fits from a $\beta \neq 1.5$ indicates that the scaling factor can be neglected at least for the purposes of this initial study. Moreover, the uncertainty introduced is expected to be negligible, even for the more important case of growth to C = bulk metal (see the x_{growth} values in ref 46 elsewhere[2]), especially in comparison to the uncertainties discussed in the present paper (Table 1) resulting from curve fitting for four rate constants in an overall five-dimensional space.

(22) (a) The ~1200 average is certainly an approximation: the metal atoms formed last will obviously produce less cyclohexane than those formed first. However, the justification of this approximation is supported by several facts: first, the metal atoms do not remain active during the full reaction; instead, they are covered by another layer of atoms and thereby become inactive. Their lifetime distribution (and hence the distribution of the number of catalytic cycles for any one atom) is consequently narrowed. Second, the errors involved are expected to be negligible in comparison to those from the curve fits in an overall five-dimensional space (i.e., see Table 1). And third, any resultant uncertainty introduced is small relative to the inherently lower precision and larger errors in such macromolecule measurements.[30]

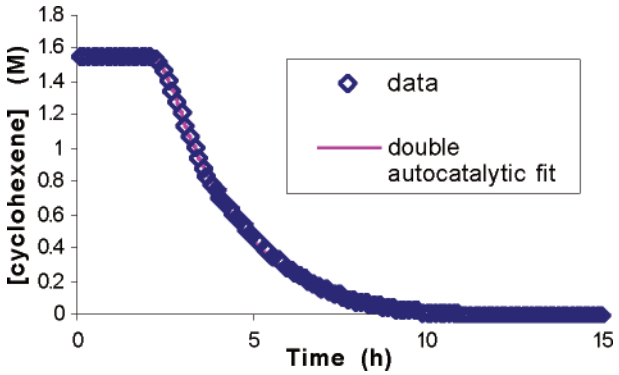

Figure 5. A typical curve fit of a (1,5-COD)$PtCl_2$ reduction curve and concomitant cyclohexene hydrogenation with the double autocatalytic mechanism in eqs 3a−3d and Scheme 3 accomplished via the use of the pseudo-elementary step treatment, eqs 5a−5d, 6a, and 6b. The k_1-k_4 rate constants from the curve fit to this specific data set are listed in Table 1 as trial #1.

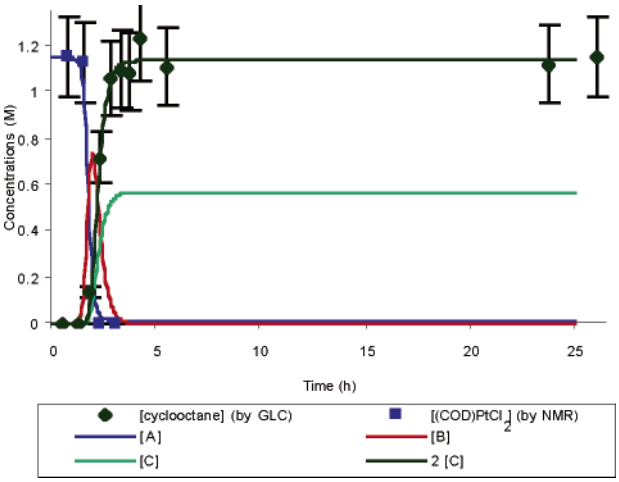

Figure 6. ^1H and GLC monitoring of the (1,5-COD)$PtCl_2$ precursor. The observed kinetic curves for (1,5-COD)$PtCl_2$ loss, and for cyclooctane formation, are well-fit by the double autocatalytic mechanism and the resultant k_1-k_4 rate constants fall within the range of values obtained via the cyclohexene reporter reaction. These results therefore provide confidence in the indirect—but easily applied and powerful—cyclohexene reporter reaction kinetic method employed herein. Note that the 2[C] line is the one that correlates with the observed data (not the 1[C] line which is shown only for comparison purposes), as expected since the A/C (equals the B/C) stoichiometry is 2/1 as eq 5d details.

albeit only one point every 20 min. *The resultant, combined* ^1H NMR and GLC data are well-fit by the proposed mechanism, Figure 6. No cyclooctadiene or cyclooctene intermediates were detected by GLC. As before,[2] the mathematics detailed in the Supporting Information teach that the ^1H NMR and GLC data provide k_i values *directly* rather than as their corresponding k_{obs} values (i.e., no 1200 correction factor is present as is the case for the indirect cyclohexene reporter reaction, eq 7, vide supra). The GLC-derived k_i parameters all lie within the range of k_1-k_4 values derived from the cyclohexene hydrogenation reporter reaction studies as the data in Table 1 documents, vide infra.

The above GLC and NMR studies are a testament to the power of the cyclohexene reporter reaction kinetic method and the more than 700 kinetic experiments this method has allowed:[2,3,7−9,11,13] it is much easier to perform and also provides 1500 high ($\leq\pm$0.01 psig) precision data points from the H_2 pressure transducer (cf. the 11 total data point of ±10% precision obtained by GLC). It is no accident,

Scheme 4

A → B
A+B → 2B
2B → C
A + C → 1.5C

Scheme 5

A → B
B +B → C
B + C → 1.5C
A + C → 1.5C

therefore, that the cyclohexene reporter reaction and pseudo-elementary step treatment is responsible for a large part of what is firmly and quantitatively understood about the mechanism of transition-metal nucleation, autocatalytic surface growth, and agglomeration from metal salts placed under reductive conditions.[2,3,7,13]

(5) Fifteen Alternative Mechanisms That Were Excluded Experimentally. Since no mechanism can ever be proven but, instead, alternative mechanisms can only be disproved, it was crucial that we spent extensive time and effort trying to fit our data with all conceivable alternative mechanisms that were even remotely reasonable. This is especially true since there are four adjustable parameters (i.e., the four k_1-k_4 rate constants) in the curve fits.[23] Hence, 15 alternative mechanisms were conceived, tested and ruled out. A few of the most important alternative mechanisms are listed below; the others are provided in the Supporting Information.

Back in Figure 4 we showed that the two-step mechanism,[2] A→B, A + B → 2B, and the three-step mechanism,[3] which includes the 2B→C agglomeration step, provide very poor fits; hence, they can be discarded. Among the 13 additional alternative mechanisms examined, the two shown in Schemes 4 and 5 are of particular importance. Both include the key feature of *double autocatalysis*, both employ bulk metal (C) as the catalyst, and both provide fits with as low a residual as the proposed mechanism displayed back in eqs 3a−3d and Scheme 3 (Figures S-3 and S-4 of the Supporting Information). The important question of how the mechanisms in Schemes 4 and 5 were ruled out is addressed next.

The alternative mechanism in Scheme 4, where the fourth step of A + C → 1.5C replaces B + C → 1.5C in the proposed mechanism, addresses the issue: "If bulk metal, C, is the kinetically dominant catalyst for *cyclohexene* hydrogenation, can it also be the dominant catalyst for the reduction of the *precursor*, *A*?"

To address this question, we calculated concentration vs time profiles for the two mechanisms shown in Figure 7 by

(23) The examples in the main text show that even a very good fit to a large amount of high-precision kinetic data is not enough to ensure the correct mechanism has been uncovered when one has four adjustable rate constants. Additional data is needed, and the true mechanism must be able to explain *all* of that data.[11] In the present case this means that just following via our cyclohexene reporter reaction only one species (i.e., C), out of the three chemically important species (A, B, and C), is insufficient to distinguish mechanisms which display different curves for A and B, yet show very similar behavior for C as a function of time. This is why experiments such as the NMR detection of A vs time reported in the main text are crucial, even though those experiments provide a very limited amount of data for curve fitting.

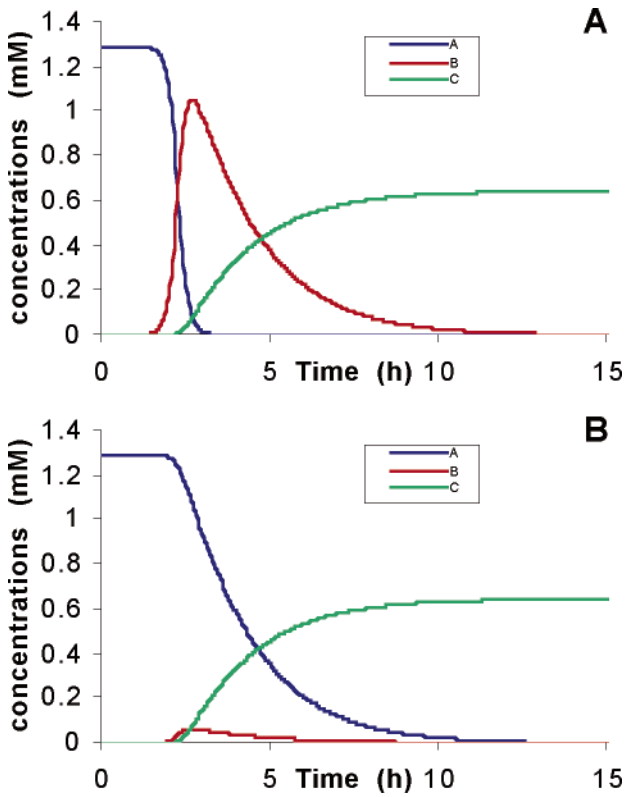

Figure 7. Calculation of the concentrations of A ((1,5-COD)$PtCl_2$), B (nanoclusters), and C (bulk metal) with the mechanism A → B, A + B → 2B, 2B → C, X + C → 1.5C, X = B (Figure 7A) or X = A (Figure 7B).

inputting the rate constants, derived from each of the respective fits to the experimental data, into the GEAR numerical integration feature of MacKinetics. Those curves reveal that the main difference between these the proposed mechanism (with B + C → 1.5C as the fourth step), vs the alternative mechanism (with A + C → 1.5C as the fourth step), is whether or not B builds up: B reaches significant concentrations in the proposed mechanism, but does not build up appreciably in the mechanism with A + C → 1.5C, Figures 7A and 7B, respectively.

The evidence ruling out the alternative mechanism with the A + C → 1.5C step, but supporting the proposed mechanism with the B + C → 1.5C step, is 4-fold and compelling: (i) TEM experiments show that nanoclusters (B) are formed in significant amounts (recall Figure 3); (ii) the transient homogeneous gray color, visible in the solution for a few moments around the end of the cyclohexene hydrogenation induction period, also indicates the presence of nanoclusters; and (iii) nanoclusters have been synthesized in experiments which feature the double autocatalytic mechanism,[12] further evidence supporting the thesis that appreciable concentration of nanoclusters are present during the (1,5-COD)$PtCl_2$ reduction reaction. In addition, even though both mechanisms are able to fit the GLC data (iv) the GLC results favor the B + C → 1.5C mechanism since only with that mechanism are k_1−k_4 rate constants obtained which lie within the range of values expected from the cyclohexene reporter reaction. Apparently, the B + C → 1.5C reaction dominates over the A + C → 1.5C one *in the present case and under our specific conditions* since B builds up fast at the end of the induction period and since A appears to be consumed before C builds up to significant concentrations. In short, the mechanism involving a dominant role for the A + C → 1.5C step can be ruled out *in the present case*.

However, our intuition is that *in the most general case both the B + C → 1.5C and A + C → 1.5C steps can probably occur*. Hence, only by employing Ockham's Razor have we written our proposed, *deliberately* minimalistic mechanism in Scheme 3 with only the B + C → 1.5C step. Noteworthy here is Carpenter and Hoffmann's caution that Ockham's Razor, a logical rule for processing experimental data via *conditional* exclusions, does not require that Nature be simple.[24]

Since two autocatalytic steps proved crucial to fitting the experimental curves, and since the mechanism with A + C → 1.5C provided a good fit to at least the cyclohexene reporter reaction kinetic curves, it became obvious that was important to examine the mechanism in Scheme 5 featuring *both* the A + C → 1.5C and B + C → 1.5C steps (i.e., but where the precedented[2] autocatalytic A + B → 2B step has been removed and replaced by the A + C → 1.5C step). Not surprisingly since it includes two autocatalytic steps, this mechanism is able to fit the kinetic data (Figure S-4 of the Supporting Information).

However, simulations carried out using the rate constants produced by fitting with this mechanism (Figure S-16) reveal that *if* the mechanism in Scheme 5 is correct, *then* A would have to react immediately with no induction period, *contrary to what is seen experimentally by NMR*, Figure 6 (vide supra). Hence, the alternative mechanism in Scheme 5 is disfavored as well.

Additional mechanisms were tested and ruled out; the details of those studies and the associated figures (Figures S-6 to S-15) are provided in the Supporting Information. The bottom line here is that our extensive examination of 15 total alternative mechanisms reveals that the proposed mechanism, eqs 3a−3d and Scheme 3, is the only mechanism we have been able to come up with which explains all the available data and which we could not exclude.

(6) Evidence for C (not B) as the Active Cyclohexene Hydrogenation Catalyst, Plus Evidence for Particle-Size-Dependent Fractional Surface Ligation of the Nanoclusters. The literature[10] as well as our prior work[2] suggests that the nanoclusters B will generally be the more active catalyst in comparison to the agglomerated bulk metal C. The facts that the nanoclusters are smaller, possess high surface area, and are less stable (less negative $\Delta H_{formation}$) and thus presumably more reactive also meant that it has generally been thought that nanoclusters will *always* be the better catalysts vs bulk metal[7]—at least up until now!

The attempt to fit our cyclohexene concentration curve by assuming that B is the cyclohexene hydrogenation catalyst proved unsuccessful, Figure S-5 of the Supporting Information. Instead, only when C is the *cyclohexene* hydrogenation catalyst are we able to obtain excellent fits to the observed kinetic data. The finding that the nanoclusters are *not* the

(24) Hoffmann, R.; Minkin, V. I.; Carpenter, B. K. *Bull. Chem. Soc. Fr.* **1996**, *133*, 117.

dominant *cyclohexene*[25] hydrogenation catalyst in this system, but that C is, instead, and under our specific conditions, was unexpected.

However, a bit of reflection yields an important hypothesis here: the normally coordinatively unsaturated, catalytically active nanoclusters appear to have been poisoned by the nanocluster-binding Bu_3N and/or Cl^- ligands that are present. Bulk metal particles C, on the other hand, apparently have a lower affinity for those same ligands so that they are able to dissociate a greater fraction of those ligands,[26a] thereby achieving a higher degree of coordinative unsaturation as required for reasonable catalytic activity. That is, a *particle-size-dependent fractional surface coverage* is indicated here, with bulk metal having more open, active sites than smaller nanoclusters. This finding, that larger particles apparently dissociate a greater fraction of their surface ligands, could simply be a greater steric effect of bulky ligands such as Bu_3N on flat, bulk metal vs curved nanoparticle surfaces, a phenomenon that has good precedent.[26] The other way to state this (i.e., the other hypothesis possible here) is that nanoclusters appear to have particle-size-dependent metal-ligand BDEs[12]—a statement which may be more correctly stated as *nanoclusters appear to have coverage-dependent, average BDEs that are a function of nanocluster size*.[26] A search of the literature reveals a (single) precedent in support of this latter hypothesis: a paper reporting metal-ligand BDEs that are $\sim^1/_2$ as strong for bulk metal in comparison to nanoclusters of the same metal.[26h] Whatever the best explanation (which is important and will require more investigation), *the observation that the larger particles are the catalyst when an excess of good ligands are present has many important implications for the design and execution of future, size-dependent catalysis and other nanocluster studies*.

The type and amount of added ligands promise, therefore, to be a key in determining when the new mechanism in Scheme 3 "turns on". We are investigating further the effects of different ligands, their concentrations, temperature, stirring rates,[27] and other variables as part of an extensive survey to determine the factors which have the greatest influence on the four-step, double autocatalytic mechanism.[28] We have already shown elsewhere[12] that the addition of 44 equiv of pyridine does, in fact, turn the normally two-step mechanism seen for our Ir nanocluster system and its sigmoidal kinetic curve (as seen back in Figure 1) into the four-step mechanism with its quite different, step-function-like kinetic curve.

(7) Searching for the Global Minimum in a Five-Dimensional Space Using MacKinetics. MacKinetics or its PC predecessor has been used in our laboratory since the early 1990s for fitting curves to the then two-step, A → B, A + B → 2B mechanism[2] and, more recently, the three-step mechanism with its added B + B → C step.[3] Those previous fits involve a maximum of three rate constants plus the residual, that is, a total of four adjustable parameters. We use MacKinetics because it is one of few kinetics packages that allow curve fitting,[29] as opposed to just simple numerical integration simulations, as well as stoichiometry factors that are not just integers (i.e., the B + C → 1.5C

(25) Note that the A + B → 2B step is required to obtain good curve fits (and is, therefore, a step in the proposed mechanism in Scheme 3); that is, B is the dominant catalyst for *the reduction of A* in the present system (consistent with the relatively large k_2 rate constant in Table 1 which refers to the reduction of A). The alternative mechanism in which A + B → 2B in Scheme 3 is replaced by A + C → 1.5C, but in which B + C → 1.5C is still present, was tested and can be ruled out as detailed in the main text in the section on "Alternative Mechanisms That Were Experimentally Excluded". The implication here is that the higher early concentration of B compared to C allows the A + B reaction to dominate kinetically early in the reaction. Conceivable differences in the mechanism for the reduction of A (=(1,5-COD)$PtCl_2$, with its site of coordinative unsaturation) compared to the mechanism of cyclohexene reduction may also be at work here.

(26) (a) Higher surface coverage for the smaller nanoclusters with their curved surface, vs flatter metal particles, for bulky ligands such as Bu_3N may be another factor here,[26b−e] one that we intend to check experimentally via future studies. That is, the apparent, average bond energy increase with decreasing size may at least in part be due to a change in the fractional surface coverage as a function of size.[26b−e] It is certainly well-known that ligand binding to metal surfaces varies as a function of the extent of coverage[26c−f] and that steric effects are higher on flat surfaces than on the highly curved surfaces of smaller nanoclusters.[26b,e] (b) Leff, D.; Ohara, P. C.; Heath, J. R.; Gelbart, W. M. *J. Phys. Chem.* **1995**, *99*, 7036; see for example Figure 2 therein. We thank a referee for this reference and for their input on this important point. (c) Weinberg, H. *Survey Prog. Chem.* **1983**, *10*, 1−59; see Figure 23. (d) Neurock, M.; Pallassana, V.; van Santen, R. A. *J. Am. Chem. Soc.* **2000**, *122*, 1150. (e) Templeton, A. C.; Hostetler, M. J.; Kraft, C. T.; Murray, R. W. *J. Am. Chem. Soc.* **1998**, *120*, 1906. (f) Varushchenko, V. M.; Polkovnikov, B. D.; Bogdanovskii, G. A.; Akimov, V. M. *Izv. Akad. Nauk SSSR, Ser. Khim.* **1972**, *7*, 1662. (g) Interestingly, a SciFinder search of "decreasing heats of adsorption with increasing surface coverage" yielded 66 hits, suggesting the greater generality of this phenomenon, although many of the references were on systems other than ligands attached to transition-metal surfaces. (h) Parks, E. K.; Nieman, G. C.; Kerns, K. P.; Riley, S. J. *J. Chem. Phys.* **1998**, *108*, 3731.

(27) (a) S*tirring effects* are known from Epstein's seminal work[27b] to have dramatic effects on the level of reproducibility of systems involving autocatalytic reactions, A + B → 2B (i.e., where B is both a reactant and a product so that as the reaction proceeds, it goes faster and faster, with a diagnostic, often sigmoidal shape in the case of single autocatalysis[2,3,7−9,11,13]). The classic case in point is the chlorite-thiosulfate, $ClO_2^- - S_2O_3^{2-}$, "clock" reaction.[27b] Epstein notes that[27b] "Careful efforts to remove all the sources of variability among (repeat) experiments met with *total failure* {italics have been added}. Despite elaborate schemes to ensure that all experiments were the same with regard to temperature, initial concentrations, exposure to light, vessel surface, age of solutions, and mixing procedure, the reaction times still varied over a wide range". The point relevant to the present Pt^0 formation paper is that the observed ≤±100% variability in the length of the induction period, for example, is probably *very small* compared to most other nanocluster systems, due to the following: (i) our awareness of Epstein's work and thus our attempt to employ uniform stirring—albeit always imperfect stirring, as Epstein notes;[b] (ii) the use of the well-defined, pure, reproducible precursor, (1,5-COD)$PtCl_2$; and (iii) our knowledge of and strict control over the reaction vessel (i.e., the use of a new culture tube liner and stir bar for each experiment to prevent undesired heterogeneous nucleation)[2] and over the acetone solvent source, its impurities, and its water content (variables known since 1994 to have large effects on the induction period[11b]). Hence, the important conceptual point here is that error bars of ≤±100%, which are large by small-molecule standards and which are the only and thus the *state-of-the-art results*, are probably actually *small* by larger molecule standards[30] (i.e., cf. the up to 5-fold greater *R* value for a protein single-crystal structure vs a small molecule *R* value). They may also prove to be relatively small error bars for reactions involving *two autocatalytic steps*. (b) Epstein, I. R. *Nature* **1995**, *374*, 321.

(28) Finney, E. E.; Finke, R. G. Unpublished results and experiments in progress.

(29) The other available kinetic packages that allow fitting are, as far as we have been able to discern: Gepasi (http://www.gepasi.org), the package Kinsim/Fitsim (http://biochem.wustl.edu/cflab/message.html), ZiTa (http:// www.staff.u-szeged.hu/~peintler/index.html), and Dynafit (http:// uwmml.pharmacy.wi.sc.edu). Additional information is provided in the Supporting Information. We are working with the author of Dynafit to see if that promising package cannot be customized to be more useful for treating nonbiological problems (e.g., where the ability to treat fractional coefficients for rate equations, as seen herein, will be possible).

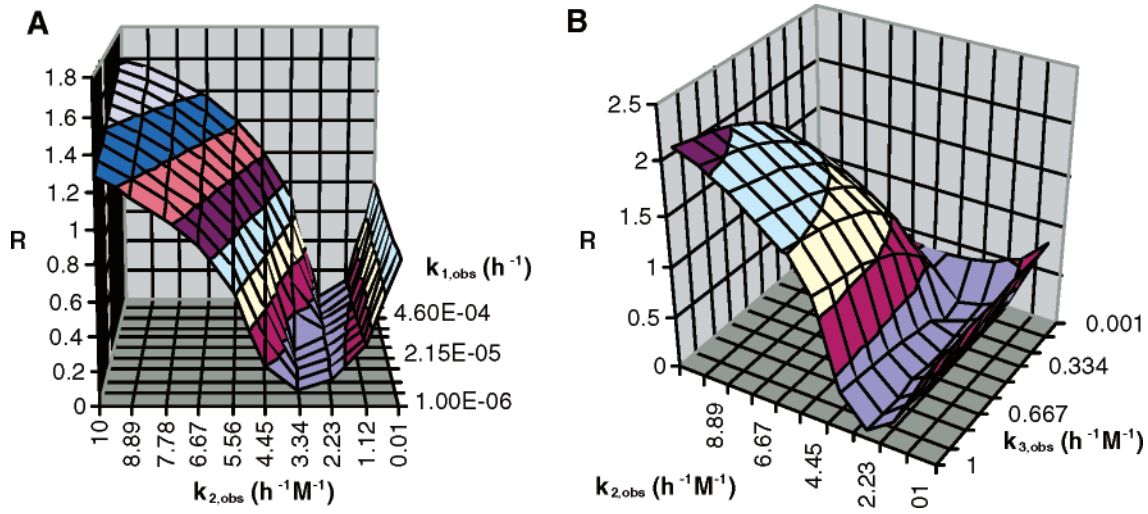

Figure 8. Two (of 600 possible) three-dimensional maps of the residual vs parameters surface calculated from a grid search carried out on a standard (1,5-COD)$PtCl_2$ reduction reaction (R = residual). The best, grid-search-determined values of the two fixed parameters (k_3 and k_4, Figure 6A, and k_1 and k_4, Figure 6B) were used in constructing these graphs.

step). MacKinetics is also relatively easy to use and has generally proved robust in our experience. A short highlight of the alternative kinetics packages that are available is provided in the Supporting Information, documentation that will make it even more apparent why we use MacKinetics, at least at present.[29]

In the present work we are searching for four parameters plus the residual, that is, for *five total* unknowns. Although we have lots of high-precision ($\pm \leq 0.01$ psig H_2 pressure) data, and even though the ratio between the numbers of data points and unknown parameters is high (≥ 100), looking for the true global minimum in a five-dimensional space was expected to be,[18] and has proved to be, tedious work at the limit of MacKinetics' capabilities. Further details of how the problems escalate dramatically as the number of steps in the mechanism, and hence the unknown rate constants, increase are detailed in the Supporting Information.

Overall, a blind search for the minimum proved unreliable in the case of the four-step mechanism with its five dimensions. A general "mapping" of the surface proved necessary and was accomplished by performing multiple grid searches. When this method is used, becoming trapped in local minima is less likely, and the best residual found should be close to the global minimum. Even the possibility of an unlucky fall into a local minimum can be excluded by conducting different grid searches and verifying that they give similar results—so that is precisely the tactic that was used in the present studies.

Grid searches can also be used to draw the multidimensional map of the surface. Of course, since only three dimensions can be displayed at once (Figure 8), any representation of the resulting five-dimensional map will always be incomplete. However, mapping the surface still yields good insights into the global structure of the surface near its global minimum. As an instructive example, the maps where k_1 varies were constructed and viewed. A valley parallel to the k_1 axis is observed, Figure 8A. It is not surprising, then, that MacKinetics has difficulties finding the minimum in this dimension since even a large variation of the parameter induces only a slight variation of the residual. The range of values found for k_1 varied *by over* 8 orders of magnitude**,** from 10^{-11} to 10^{-3} h^{-1} (see the data in Table 1, vide infra). This wide range of k_1 values was verified in the simulations to be presented shortly: variations of k_1 by even 10 orders of magnitude have little effect on the resultant kinetic curves. Physically, *this observation makes sense*: the first, slow continuous nucleation reaction, A → B, produces a negligible amount of B compared to the second autocatalytic reaction, A + B → 2B.

(8) Curve Fit k_1-k_4 Kinetic Parameters, Resultant Error Bars, and Examination of Experimental Sources of Error. Table 1 shows the observed rate constants obtained from three different repetitions of the standard (1,5-COD)-$PtCl_2$ experiment (selected as representative from the 29 total experiments).

First, it is important to note that some of the error seen in the rate constants is undoubtedly experimental in origin. The observed variability in the length (time) of the induction period of 0.4−3.0 h (average of 1.4 h; the distribution of the induction periods in our 29 experiments are summarized in Figure 9) is actually less than the factor of $\pm 10^{1.2}$ seen over a 7 year period in multiple researchers' hands (see p 10 304 elsewhere[9]) for the kinetically best-studied, and kinetically most proven reproducible, transition-metal nanocluster formation system and its two-step mechanism,[2,3,7,8] the polyoxoanion- and Bu_4N^+-stabilized Ir^0 nanoclusters formed from $(Bu_4N)_5Na_3[(1,5\text{-COD})Ir{\cdot}P_2W_{15}Nb_3O_{62}]$.

It is known that the induction period in the Ir^0 nanocluster formation reactions is very sensitive to trace water, an unidentified impurity in the acetone solvent,[11] as well as to any component of heterogeneous (solid-surface) nucleation.[9] In seminal work Epstein has shown that the effects of *always-imperfect* stirring[27] can be enormous in reactions involving autocatalysis,[27] so that one might expect even larger effects of imperfect stirring in the present case of *double autocatalysis*. Also, we have discussed elsewhere reflection on literature data teaches that larger molecule, multistep reactions such as (1,5-COD)$PtCl_2$ → $^1/_n Pt^0{}_n$ (that necessarily must involve ≫2200s of steps for $n = 2200$ and corresponding to, for example, the observed 40 Å Pt^0 nanoclusters) will

Table 1. Range of Parameters Obtained by Curve Fitting the Cyclohexene Hydrogenation Reporter Reaction Data with the Double Autocatalytic Mechanism to Three Repetitions of the Standard Conditions (1,5-COD)$PtCl_2$ Reduction Reaction[a]

rate constant	trial #1[b]	trial #2[c]	trial #3[d]	range or average	k (corrected)[e]	GLC-derived k
$k_{1,obs}$ (h^{-1})	$10^{-11}-10^{-3}$	$10^{-7}-10^{-5}$	10^{-6}	$10^{-11}-10^{-3}$	$10^{-11}-10^{-3}$	$10^{-13}-10^{-6}$
$k_{2,obs}$ ($h^{-1}\,M^{-1}$)	6 ± 3	8−11	2.5	2−11	1200−13200	800−14440
$k_{3,obs}$ ($h^{-1}\,M^{-1}$)	0.69 ± 0.04	0.10 ± 0.01	0.15	0.1−0.7	120−840	700−1200
$k_{4,obs}$ ($h^{-1}\,M^{-1}$)	0.16 ± 0.03	0.17 ± 0.01	0.15	0.16 ± 0.03	160−230	12−3600

[a] The GLC-derived results are also included in the table for comparison; note that the mathematics (provided in the Supporting Information) requires that the GLC-derived rate constants should not be corrected by the 1200 factor that is, however, required for the cyclohexene reporter reaction-derived k_{obs} values. [b] Following the procedure detailed in the Experimental Section, a total of 34 different visually good and R(residual) ≤ 0.01 curve fits were carried out for this prototype data set (i.e., and using multiple different initial guess and grid search methods). [c] A total of 4 visually good and R(residual) ≤ 0.01 curve fits were carried out for this data set. [d] A total of 2 visually good and R(residual) ≤ 0.01 curve fits were carried out for this data set. [e] The k_2-k_4 values are corrected by the mathematically required statistical factor of 1200 introduced by the cyclohexene reporter reaction stoichiometry of 1200 equiv of cyclohexene to 1 equiv of (1,5-COD)$PtCl_2$ (see eqs 5−7 and the derivations provided in the Supporting Information).

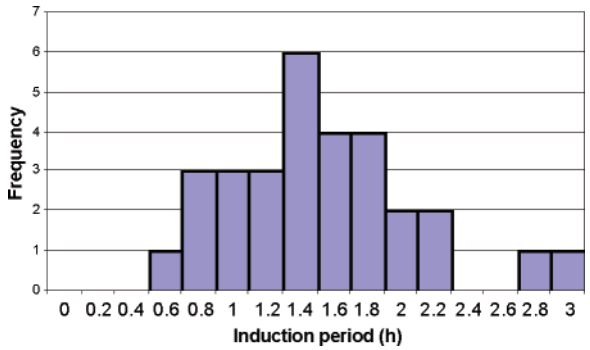

Figure 9. Distribution of the length of the induction period among the 29 experiments carried out for the (COD)$PtCl_2$ reduction and concomitant cyclohexene hydrogenation reporter reaction.

have larger error bars for most measurements[30] in comparison to their better known smaller molecule counterparts where errors of, say, ≤±15% might be common−especially when *polydisperse* products result. And, the flat surface and the inherent large error in the determination of k_1 (and as the data in Table 1 document) have already been noted. Finally, in light of the inherent uncertainties in the rate constants, the errors introduced by the approximations underlying the pseudo-elementary step (as summarized in ref 22 elsewhere[3]) should be negligible and no attempt has been made to correct for the changing fraction of surface atoms during the reaction (i.e., the "scaling factor" detailed elsewhere[2] which deals with the fact that the growth step is really[21] $Pt(0)_n + Pt \rightarrow Pt(0)_{n+1}$ and not the *idealized* $A + B \rightarrow 2B$).

In the end, the uncertainties in k_1 of even $10^{\pm 4}$, and the uncertainties of factors of 5−7 in the k_2-k_4 values, are neither surprising nor disturbing. One fact is for certain regarding the rate constants listed in Table 1: this is the first report of the four-step mechanism and derivation of four rate constants from a rather large amount (200−1500 data points) of very high precision (≤±0.01 psig) pressure data. Hence, the present work defines the *experimentally observed, present state-of-the-art error limits* to which we and others can aspire to better, *if* that proves possible and *if* better error limits become important in some application or situation.

(9) Resultant Insights. Studying Table 1 yields the following insights for the (1,5-COD)$PtCl_2$/2 Bu_3N/2 Proton Sponge system, insights which are valid even with the available precision rate constants: (i) k_1 is small, but nonzero, as some homogeneous nucleation is required to convert some $A \rightarrow B$ so that the subsequent autocatalytic steps can ensue; (ii) k_2 (for the $A + B \rightarrow 2B$ step) is about an order of magnitude or more larger than either k_3 or k_4; and (iii) k_3 and k_4 are of similar size.[31] There are several other insights that follow from the simulations provided below.

(10) Predictive Simulations Made with the New, Double Autocatalytic Mechanism. To test the predictive abilities of our model, we used it to simulate the concentrations of A, B, and C over the course of the reaction as the rate parameters or the initial concentration was varied. As already mentioned, variations of k_1 over a range of 10 orders of magnitude do not affect the shape of the curves, and only slightly change the length of the induction period. One might have expected nanocluster formation to be hypersensitive (i.e., chaotic) to the initial value of k_1; *in fact, the kinetic curves are ultra-insensitive to the* $A \rightarrow B$ *step rate constant*. An increase in k_2 shortens the induction period and increases the maximum concentration of nanoclusters. It also affects the shape of the edge of the curve−the smaller the value of k_2, the smoother the curve, the larger the value of k_2, the sharper the onset of the curve—although really sharp-starting curves such as the classic Pt^0 colloid examined elsewhere[12] do require the full four-step mechanism for the best fit. As

(30) See p 27 and ref 4 elsewhere for a discussion of the loss of precision observed in many macromolecule or materials systems and where one is measuring a collective or bulk property, and especially if the resultant material contains some *polydispersity*: Finke, R. G. Transition Metal Nanoclusters. In *Metal Nanoparticles, Synthesis, Characterization and Applications*; Feldheim, D. L., Foss, C. A., Jr., Eds.; Marcel Dekker: New York, 2001.

(31) (a) Our finding that k_3 and k_4 are ca. the same size is by itself an important finding. It stands in contrast to the (unquantitated) claim in polymer and sol-gel systems[31b,c] that smaller plus smaller particle agglomeration is less important than larger plus smaller particle aggregation. It remains to be determined if the different systems (our transition-metal vs those polymer and sol-gel systems) is the reason for the different findings or, perhaps, if our quantitated results are simply more (or less) reliable. Note that a close inspection of the sol-gel work makes apparent the difficulties of doing reliable kinetic and mechanistic studies on macromolecular, self-assembly systems. The sol-gel work is very careful work that went to great effort to employ three separate kinetic methods (conductance, volume change, and ^{29}-Si NMR) to acquire rare kinetic data for a self-assembly system. However, that work is deductive (primarily fits one assumed, theory-derived mechanism to the data) rather than being inductive (i.e., ruling out multiple, alternative specific hypotheses to get to the more general mechanism; it does rule out a diffusion-controlled mechanism, however). In the final analysis the sol−gel work[31b,c] cannot supply even a single, complete mechanism with elementary or pseudo-elementary steps and rate constants (mostly a "word mechanism" is used instead, which is typical of proposed mechanisms since the time of LaMer's work[6] as discussed briefly elsewhere[2]). Clearly, kinetic and mechanistic studies of self-assembly materials syntheses presents a generally quite difficult challenge. (b) Bogush, G. H.; Zukoski, C. F., IV. *J. Colloid Interface Sci.* **1991**, *142*, 1; see also refs 5, 36, and 37 therein. (c) Bogush, G. H.; Zukoski IV, C. F. *J. Colloid Interface Sci.* **1991**, *142*, 19.

expected, changing k_3 has little effect on the concentration of A vs time. However, with higher k_3 values, the maximum concentration of nanoclusters B decreases and they also disappear faster, increasing the rate of bulk metal C formation and exhibiting more and more step-function-like cyclohexene hydrogenation curves, all as one might intuitively expect.

Variations of the fourth parameter k_4 affect only the last part of the reaction, the formation of bulk metal. Even the edge of the cyclohexene hydrogenation curve (or, equivalently, the bulk metal (C) formation curve) is not affected, k_4 influencing predominantly the curvature at later times. Variation of the initial concentration of the precursor A is, as far as the relative positions of the resultant A, B, and C curves are concerned, equivalent to changing k_2, k_3, and k_4. The smaller the initial concentration of A, the broader the nanocluster peak, and the longer the nanoclusters stay in solution before agglomeration (as makes sense given that the nanoclusters agglomeration steps are all bimolecular). Consequently, *synthetic efforts aimed at preparing and isolating nanoclusters are best surveyed as a function of concentration and, in general, at a lower initial concentration of the precursor A.*

(11) Verification of the Mechanistic Prediction That the Use of Lower Concentrations of A, and Higher Temperature, Will Change the Selectivity to Nanoclusters Rather Than Bulk Metal. This project originally grew out of our attempts, and frustrations, at making Pt^0 nanoclusters. More than 100 experiments were conducted over a good fraction of a year while examining what we then thought was the key issue of finding the magic stabilizer for Pt^0 (from a list of premier stabilizers such as HPO_4^{2-}, the "Gold Standard" anionic stabilizer (the $P_2W_{15}Nb_3O_{62}^{9-}$ polyoxoanion[32]), to other accepted stabilizers such as Cl^-, Br^-, PVP (poly(vinylpyrrolidone)), 1,10-phenanthroline, and acetate, plus combinations of these stabilizers). All these experiments—conducted with a 1.2 mM solution of (1,5-COD)$PtCl_2$ at 22 °C and primarily in acetone—*failed;* bulk Pt^0 metal was invariably the end product.

However, as soon as the discovery of the four-step, double autocatalytic mechanism in eq 3 and Scheme 3 was available along with the insights from the simulations described above, the mechanistic prediction was made that lower concentrations of precursor and higher temperatures should favor nanocluster over bulk metal formation since these conditions should favor the unimolecular k_1 step over the bimolecular agglomeration, k_3 and k_4, steps.[12] The experimental verification of this prediction[12] proved almost "magical" in our hands: simply by *halving* the concentration of (1,5-COD)-$PtCl_2$ to 0.6 mM and by working at the higher temperature[33] of 60 °C (while also working in the higher boiling, higher dielectric constant and better stabilizing solvent propylene carbonate), we were able to obtain a solution of nanoclusters with *no* detectable bulk metal in just a *single* additional experiment![12] The magic we were searching for was contained in the mechanism, not necessarily in the choice of stabilizer! While the full details of our synthesis and characterization of Pt^0 nanoclusters will be described in due course,[34] the important point here is the striking predictive power of the double autocatalytic mechanism!

Conclusions, Caveats, Unanswered Questions, and Hence, Future Research

During the course of attempting to prepare Pt^0 nanoclusters, we discovered the unusual step-function-like curves shown in Figures 2, 4, and 5. An exhaustive search for mechanisms that might fit these curves led to the strict requirement for *two autocatalytic steps* in any proposed mechanism. The proposed mechanism in its most general form adds the step $X + C \rightarrow 1.5C$ (X = B or A) to our prior work uncovering the[2,8,9,11] $A \rightarrow B$, $A + B \rightarrow 2B$, and[3] $B + B \rightarrow C$ steps. *The overall, four-step, double autocatalytic* mechanism shown in Scheme 3 is the presently most general mechanism by which transition-metal nanoclusters nucleate, grow, and then agglomerate into bulk metal under reductive conditions. It is a mechanism fortified by a foundation of work[2,3,7−9,11] that began more than a decade ago.[11] The data for the present system are fit only by the mechanism with the $B + C \rightarrow 1.5C$ step, eq 3d, but we anticipate the possibility that the $A + C \rightarrow 1.5C$ step may be applicable in *other* systems and in general.

The full details of the kinetics treatment, the MacKinetics curve fitting, and the issues of searching for a global minimum in a five-dimensional space were also detailed so that others can optimally and efficiently exploit this work while avoiding a steep learning curve. The resultant rate constants k_1-k_4, and the implications they contain even given their stated precision, were discussed as well as the insights resulting from simulations possible using the new mechanism.

Important, more general insights resulted from this work as expected for any new mechanism, notably, the insight that one should employ lower concentrations and higher temperatures to favor the synthesis of nanoclusters rather than bulk metal; the insight that the opposite set of conditions should be used if the deposition of a bulk metal film for some application is desired; the insight that many if not most claimed Pt^0 nanocluster synthesis systems are very likely also producing bulk metal;[35] and the insight of particle-size dependent reactivates, fractional ligation, and at least apparent metal-ligand bond-dissociation energies, as well as the catalytic implications of these—namely, that nanoclusters will not have the higher catalytic activity in the presence of at least certain ligands. A search of the relevant self-assembly

(32) (a) Özkar, S.; Finke, R. G. *J. Am. Chem. Soc.* **2002**, *124*, 5796. (b) Özkar, S.; Finke, R. G. *Langmuir* **2002**, *18*, 7653. (c) Özkar, S.; Finke, R. G. *Langmuir* **2003**, *19*, 6247.

(33) It has been known for some time from the semiconductor nanoparticle literature that the use of higher temperatures favors the typically more enthalpically demanding[33c] nucleation over growth steps: (a) Murray, C. B.; Norris, D. J.; Bawendi, M. G. *J. Am. Chem. Soc.* **1993**, *115*, 8706. (b) Katari, J. E. B.; Colvin, V. L.; Alivisatos, A. P. *J. Phys. Chem.* **1994**, *98*, 4109. (c) Strey, R.; Wagner, P. E.; Viisanen, Y. *J. Phys. Chem.* **1994**, *98*, 7748.

(34) Finney, E. E.; Finke, R. G. Unpublished results and experiments in progress.

(35) Exceptions where such Pt or Pd quantitation is performed are as follows: (a) Reetz, M. T.; Helbig, W. *J. Am. Chem. Soc.* **1994**, *116*, 7401. (b) Moiseev, I. I.; Rudy, R. I.; Cherkashina, N. V.; Shubochkin, L. K.; Kochubey, D. I.; Novgorodov, B. N.; Kryukova, G. A.; Kolomiychuk, V. N.; Vargaftik, M. N. *Inorg. Chim. Acta* **1998**, *280*, 339.

literature[36,37] reveals that the mechanism detailed in Scheme 3 appears to be the largest, most complex self-assembly system that is the best understood, largely since it is supported by extensive kinetic studies that are often hard to accomplish[31a] for self-assembly reactions.

Many unanswered questions remain, however, so that there is ample room for future research. One unknown is exactly what are the full range of factors affecting k_1-k_4 and thus the mechanism in Scheme 3? We know from our in-progress[28] studies of (to date) 25 different conditions (examining 4 metals, 2 temperatures, 2 solvents, 2 ligands, and at varied concentrations) that the mechanism in Scheme 3 is very sensitive to the exact conditions. What are the most sensitive variables and why? Added ligands are clearly one key—and perhaps the key—variable. But, which ligand *and* metal combinations favor the mechanism in Scheme 3? We have seen this mechanism so far for Pt, Ir, and Ru and in one complex of Pd.[28] The temperature dependence, $\Delta H^{\ddagger}$ and $\Delta S^{\ddagger}$ for the four steps in Scheme 3 need to be determined and should prove useful ($\Delta H^{\ddagger}$ and $\Delta S^{\ddagger}$ for the first two steps in Scheme 3 in the case of Ir(0) nanoclusters are available[2a]).

Using the insights in Scheme 3 to improve literature reports of classic nanoparticles and colloids should also prove useful as has already been proven true[12] in the case of a classic preparation of Pt^0/PVP colloids.[10] Our results also promise to provide the most direct way presently available to measure nanocluster stability via quantification of the rate constants for agglomeration (k_3 and k_4 herein, vide infra), *if* suitable precision and accuracy in the curve-fit k_3 and k_4 can be obtained, a major challenge. A method that tests and quantitates the myriad of anions, polymers, dendrimers, solvents, cations, and other species claimed in the literature to be nanocluster stabilizers, but which remains unevaluated in any quantitative way due to the paucity of methods[32] to probe the relative efficacy of such claimed stabilizers, would be a valuable addition to nanocluster literature. It is these studies that promise to occupy much of our time and, we hope, the time of others interested in the self-assembly synthesis of transition-metal nanoparticles and metal films or the broader topic of self-assembly in general.[36,37]

Acknowledgment. Prof. T. Don Tilley and his group at U. C. Berkeley are thanked for a collaboration that piqued our interests in the problems synthesizing and, hence, the mechanism underlying Pt^0 nanocluster formation and agglomeration. Support from DOE Grant DE-FG02-03ER15453 and NSF Grant 0314678 (for the research assistantship to C. Besson) are gratefully acknowledged.

Supporting Information Available: (1) XPS data; (2) Double autocatalytic mechanism and pseudo-elementary step: MacKinetics treatment; (3) Alternative mechanisms ruled out: curve fits; (4) Simulation of the A, B, and C concentration using the alternative mechanism A → B, 2B → C, B + C → 1.5C, and A + C → 1.5C with C as the catalyst; (5) General mechanism with $\alpha = 1$, $\beta \neq 1.5$: MacKinetics input; (6) Searching for the global minimum in a five-dimensional space using MacKinetics; (7) A search for other, suitable packages for curve fitting; (8) Surface mapping; and (9) Simulations: effects of varying k_1-k_4, and the initial concentration of A. Evidence against the main catalyst being some form of soluble, homogeneous Pt^{II} is provided by a Hg^0 poisoning and the other data summarized in the Supporting Information elsewhere.[12] This material is available free of charge via the Internet at http://pubs.acs.org.

CM050207X

(36) Polyoxometalate investigations are among the earliest mechanistic studies of inorganic self-assembly systems;[36a,b] our own past[2,3,11] and present[12] nanocluster systems[36c] were first reported in[11] 1994 and then in greater detail in 1997, 1998, 2001, and 2004.[2,3] Self-assembly mechanistic studies of ferritin[36d] and of small, metal template systems[37] also exist. (a) Kepert, D. L.; Kyle, J. H. *J. Chem. Soc. Dalton Trns.* **1978**, 133. (b) Errington, R. J.; Lax, C.; Richards, D. G.; Clegg, W.; Fraser, K. A. In *Polyoxometalates*; Pope, M. T., Müller, A., Eds.; Kluwer Academic Publishers: The Netherlands, 1994; pp 105−114. (c) See refs 2a,b, 3, 11, and 12 cited herein. (d) Theil, E. C.; Takagi, H.; Small, G. W.; He, L.; Tipton, A. R.; Danger, D. *Inorg. Chim. Acta* **2000**, *297*, 242.

(37) A SciFinder search reveals that kinetic and mechanistic studies of self-assembly reactions are fairly rare in any area of chemical science, despite the importance of and emphasis on self-assembly to make more complex structures and materials. Lead references to studies of small, metal-template systems are as follows: (a) Hasenknopf, B.; Lehn, J.-M.; Boumediene, N.; Leize, E.; Van Dorsselaer, A. *Angew. Chem., Int. Ed.* **1998**, *37*, 3265. (b) Fatin-Rouge, N.; Pfeil, A.; Rigault, A.; Albrecht-Gary, A.-M.; Lehn, J.-M. *Helv. Chim. Acta* **2001**, *84*, 1694. (c) Levin, M. D.; Stang, P. J. *J. Am. Chem. Soc.* **2000**, *122*, 7428. (d) Fatin-Rouge, N.; Blanc, S.; Leize, E.; Van Dorsselaer, A.; Baret, P.; Pierre, J.-L.; Albrecht-Gary, A.-M. *Inorg. Chem.* **2000**, *39*, 5771. (e) Hamacek, J.; Blanc, S.; Elhabiri, M.; Leize, E.; Van Dorsselaer, A.; Piguet, C.; Albrecht-Gary, A.-M. *J. Am. Chem. Soc.* **2003**, *125*, 1541. (f) Elhabiri, M.; Hamacek, J.; Bünzli, J.-C. G.; Albrecht-Gary, A.-M. *Eur. J. Chem.* **2004**, 51.